HHS Public Access

Author manuscript

Bone. Author manuscript; available in PMC 2016 July 27.

Published in final edited form as:

Bone. 2014 January ; 58: 177–184. doi:10.1016/j.bone.2013.07.021.

A pre-clinical murine model of oral implant osseointegration

S. Mouraret[a,b], **D.J. Hunter**[a], **C. Bardet**[a,c], **J.B. Brunski**[a], **P. Bouchard**[b], and **J.A. Helms**[a,*]

[a]Division of Plastic and Reconstructive Surgery, Department of Surgery, Stanford School of Medicine, Stanford, CA 94305, USA

[b]Department of Periodontology, Service of Odontology, Rothschild Hospital, AP-HP, Paris 7 Denis, Diderot University, U.F.R. of Odontology, Paris, France

[c]Dental School University Paris Descartes PRES Sorbonne Paris Cité, EA 2496 Montrouge, France

Abstract

Many of our assumptions concerning oral implant osseointegration are extrapolated from experimental models studying skeletal tissue repair in long bones. This disconnect between clinical practice and experimental research hampers our understanding of bone formation around oral implants and how this process can be improved. We postulated that oral implant osseointegration would be fundamentally equivalent to implant osseointegration elsewhere in the body. Mice underwent implant placement in the edentulous ridge anterior to the first molar and peri-implant tissues were evaluated at various timepoints after surgery.

Our hypothesis was disproven; oral implant osseointegration is substantially different from osseointegration in long bones. For example, in the maxilla peri-implant pre-osteoblasts are derived from cranial neural crest whereas in the tibia peri-implant osteoblasts are derived from mesoderm. In the maxilla, new osteoid arises from periostea of the maxillary bone but in the tibia the new osteoid arises from the marrow space. Cellular and molecular analyses indicate that osteoblast activity and mineralization proceeds from the surfaces of the native bone and osteoclastic activity is responsible for extensive remodeling of the new peri-implant bone. In addition to histologic features of implant osseointegration, molecular and cellular assays conducted in a murine model provide new insights into the sequelae of implant placement and the process by which bone is generated around implants.

Keywords

Dental; Histology; Maxilla; Oral cavity; Mice; Model

*Corresponding author. Fax: +1 650 736 4374. jhelms@stanford.edu (J.A. Helms).

Conflict of interest

The authors declare that they have no conflict of interest.

Supplementary data to this article can be found online at http://dx.doi.org/10.1016/j.bone.2013.07.021.

Introduction

Oral implants are considered to be very successful prosthetic devices. They successfully replace the function of teeth and restore esthetics, and do so with a remarkably low failure/complication rate. Given these appealing characteristics, it is understandable that over the last decade the demand for oral implants has risen sharply [1]. With this precipitous increase has come a staggering array of implant modifications, all designed to improve the process of osseointegration. These modifications include adjustments in the time to loading [2], variations in surface characteristics [3], alterations in implant shape [4], and the addition of growth factors or other biological stimuli intended to "activate" the implant surface [5]. The extent to which most of these modifications actually improve implant osseointegration, however, is not known. Clearly, understanding the benefits and detriments of these changes is critically important if we want to maintain the successful profile of oral implants.

Consequently, it comes as somewhat of a surprise that the vast majority of experimental studies on oral implant osseointegration are conducted in long bones, rather than on the maxilla or mandible. The most often-quoted reasons for carrying out analyses of oral implants in long bones are their relative size and easy accessibility [6–8]. Long bones also contain a very large and pro-osteogenic marrow cavity, which facilitates rapid bone formation around an implant [9,10]. Furthermore, studies that we conducted in mice demonstrate that the marrow space is primarily responsible for generating this new peri-implant bone [6,10,11]. Using an in vivo loading device, we further demonstrated that defined forces delivered to the implant in the tibia in turn produce measurable deformations [12]. Using this information we have identified principal strains in the 10–20% range to stimulate osseointegration [13,14]. Genetic mouse models have been particularly helpful in identifying key variables that influence osseointegration; namely, we demonstrated that early excessive micromotion can cause fibrous encapsulation [15] and the elimination of mechanically sensitive cellular appendages such as primary cilia can obliterate the strain-induced bone formation [16,17].

All of these studies have been conducted in the tibia. The vast majority of implants are placed in the oral cavity [18] but in experimental models the oral cavity represents a novel, nearly unexplored, and particularly challenging microenvironment for implant osseointegration. Investigators have reported on the use of rat models to study oral implant osseointegration [19,20], some with considerable success [21]. Here, we sought to extend these findings using an animal model amenable to genetic manipulation. Our goal was to recapitulate this unique milieu of implant osseointegration in the oral cavity using a mouse model, where a vast armamentarium of genetic models and molecular and cellular assays could be employed to understand and potentially improve the process of osseointegration.

Materials and methods

Animal care

All procedures followed protocols approved by the Stanford Committee on Animal Research. Wild type, male, skeletally mature (between 3 and 5 months old) CD1 mice that had an average weight of 28 g were obtained from the Jackson Laboratory (Bar Harbor,

ME). Animals were housed in a temperature-controlled environment with 12-h light dark cycles and were given soft diet food (Bio Serv product #S3472) and water ad libitum. No antibiotics were given to the operated animals and there was no evidence of infection or prolonged inflammation at any of the surgical sites.

Implant surgery in the oral cavity

Twenty-three adult mice were anesthetized with an intraperitoneal injection of Ketamine (80 mg/kg) and Xylazine (16 mg/kg). The mouth was rinsed using a povidone–iodine solution for 1 min followed by a sulcular incision (Micro angled blade 10035-15, Fine Science Tools, USA) that extended from the maxillary first molar to the mid-point on the alveolar crest until behind the incisor. A full-thickness flap was elevated; a pilot hole was made to prepare the implant bed on the crest, 1.5 mm in front of the first maxillary molar using a Ø 0.3 mm pilot drill bit (Drill Bit City, Chicago, IL), and followed with a drill bit of Ø 0.45 mm. All drill holes were made using a low-speed dental engine (800 rpm). In cases where no implants were placed, the surgical site was carefully rinsed and closed using non-absorbable single interrupted sutures (Ethilon Monofilament 9-0, BV100-3, 5 in., Johnson & Johnson Medical, USA).

In cases where an implant was placed, the titanium implant (0.6 mm diameter titanium-6 aluminum-4 vanadium alloy “Retopins”, NTI Kahla GmbH, Germany) was cut at length of 2 mm and was screwed down in the implant bed, maintained by a needle holder. A small portion of the implant was left exposed, approximating the height of the gingiva following with the standard procedure used for one-step oral implant placement. The flap was closed as described above. Following surgery, clinical examinations were performed and mice received subcutaneous injections of buprenorphine (0.05–0.1 mg/kg) for analgesia once a day for 3 days. Mice were sacrificed at 7, 14, 21 and 28 days post-surgery.

Implant surgery in the tibia

Adult wild-type mice were anesthetized as above; an incision was made over the right anterior-proximal tibia surface. Care was taken to preserve the periosteal surface. Holes were drilled through one cortex using a 1 mm drill bit (Drill Bit City, Chicago, IL). Implants were placed as described [12,14]. The skin was closed around the implant with non-absorbable sutures as described above, and pain management was followed as described above.

Sample preparation, processing, histology

Maxillae and tibias were harvested, the skin and outer layers of muscle were removed, and the tissues were fixed in 4% paraformaldehyde overnight at 4 °C. Samples were decalcified in a heat-controlled microwave in 19% EDTA for two weeks and after complete demineralization, the implant was gently removed from the samples. Specimens were dehydrated through an ascending ethanol series prior to paraffin embedding. Eight-micron-thick longitudinal sections were cut and collected on SuperFrost-plus slides for histology including Movat’s pentachrome, aniline blue, and Picrosirius red staining.

Cellular assays

Alkaline phosphatase (ALP) activity was detected by incubation in nitro blue tetrazolium chloride (NBT; Roche), 5-bromo-4-chloro-3-indolyl phosphate (BCIP; Roche), and NTM buffer (100 mM NaCl, 100 mM Tris pH 9.5, 5 mM MgCl). Tartrate-resistant acid phosphatase (TRAP) activity was observed using a leukocyte acid phosphatase staining kit (Sigma). After its development, the slides were dehydrated in a series of ethanol and xylene and subsequently cover-slipped with Permount mounting media.

For TUNEL staining, sections were incubated in proteinase K buffer (20 μg/mL in 10 mM Tris pH 7.5), applied to a TUNEL reaction mixture (In Situ Cell Death Detection Kit, Roche), and mounted with DAPI mounting medium (Vector Laboratories). Slides were viewed under an epifluorescence microscope.

Immunohistochemistry

Tissue sections were deparaffinized following standard procedures. Endogenous peroxidase activity was quenched by 3% hydrogen peroxide for 5 min, and then washed in PBS. Slides were blocked with 5% goat serum (Vector S-1000) for 1 h at room temperature. The appropriate primary antibody was added and incubated overnight at 4 °C, then washed in PBS. Samples were incubated with appropriate biotinylated secondary antibodies (Vector BA-x) for 30 min, then washed in PBS. An avidin/biotinylated enzyme complex (Kit ABC Peroxidase Standard Vectastain PK-4000) was added and incubated for 30 min and a DAB substrate kit (Kit Vector Peroxidase substrate DAB SK-4100) was used to develop the color reaction. Antibodies used include proliferating cell nuclear antigen (PCNA, Invitrogen) Osteocalcin (Abcam ab93876), Decorin (NIH LF 113), Osteopontin (NIH LF 175), Fibromodulin (NIH LF 149), and Procollagen 1(NIH LF42). Each immunostaining reaction was accompanied by a negative control, where the primary antibody was not included.

Histomorphometric analyses

Maxillas were collected on postsurgical days 7, 14, 21, and 28 to quantify the amount of new bone generated in response to the implant. All maxilla were embedded in paraffin and sectioned longitudinally. The 0.6-mm implant was represented across ∼20 tissue sections, each of which was 8 μm thick. Of those 20 sections, we used a minimum of 4 sections to quantify the amount of new bone. All the tissue sections were stained with aniline blue, which labels osteoid matrix. The sections were photographed using a Leica digital imaging system at the same magnification (×10 objective). The resulting digital images were analyzed with Adobe Photoshop CS5 software. We chose a fixed, rectangular region of interest (ROI) that in all images corresponded to 10^6 pixels. The injury site was always represented inside this ROI by manually placing the box in the correct position on each image.

The aniline blue-positive pixels were partially automated by using the magic wand tool set to a color tolerance of 60. This tolerance setting resulted in highlighted pixels with a range of blue that corresponded precisely with the histological appearance of osseous tissue in the aniline blue-stained sections. Native bone or bone fragments resulting from the drill injury were manually deselected. The total number of aniline blue-positive pixels for each section

was recorded. The pixel counts from individual sections were averaged for each sample, and the differences within and among treatment groups were calculated based on these averages.

Statistical analyses

Results are presented as the mean ± SEM. Student's t-test was used to quantify differences described in this article. $P \leq 0.01$ was considered to be significant.

Results

Neural crest-derived maxillary bone heals differently than mesoderm-derived tibial bone

The skeleton contains tissue-resident stem cells that are responsible for maintaining bone mass [22] and for regenerating new bone following injury [23]. By genetic cell lineage labeling studies [24], we established that adult skeletal stem cells arise from the cranial neural crest and the mesoderm [23]. Although both stem cell populations give rise to cartilage and bone, they do not appear to be functionally equivalent: Neural crest-derived skeletal progenitor cells, which occupy the first branchial arch (Figs. 1A,B) and give rise to the bones and cartilages of the upper and lower jaws (Figs. 1C–F) exhibit robust plasticity compared to mesoderm-derived progenitor cells, most notably in bone grafting assays [25]. Our initial hypothesis was that implant osseointegration in the tibia would be equivalent to implant osseointegration in the maxilla. Since the two bones are derived from different embryonic stem cell populations, however, we directly tested the healing potentials of the tibia compared to the maxilla.

We employed a simple bone defect model in which a 1.0 mm hole was created in a mesoderm-derived long bone, the tibia, or a neural crest-derived cranial bone, the maxilla (Figs. 1G,H). The surrounding cortices were left intact, which minimized micromotion of the injured bones. There was no obvious difference in the histologic appearance of the injury sites within the first few days of creating the defects (Fig. 1H and data not shown). By post-injury day 14, however, there was a clear distinction: tibial injuries were filled with newly woven bone that occupied the marrow cavity and bridged the defect (Fig. 1I). In contrast, a similar injury in the maxilla was filled with a fibrous connective tissue (Fig. 1J). Even if we reduced the diameter of the maxillary defects (compare 1.0 mm in the tibia with 0.5 in the maxilla), the maxillary injuries did not heal by day 14.

Are maxillary injuries just slower to heal than tibial injuries? We examined the injury sites on day 28 and found that the tibial injuries had completely healed by bony bridging (Fig. 1J), whereas maxillary injury sites remained filled with connective/fibrous tissue (Fig. 1L). Therefore, in addition to their distinct embryonic origins, and a measurable osteogenic capacity of bone grafts derived from the two skeletal elements, craniofacial and long bones have different rates of healing. We reasoned that this difference would likely manifest as a change in the rate or extent of implant osseointegration.

Establishing an oral implant procedure in mice

Our primary interest is in addressing failures in oral implant osseointegration. Given the different healing potentials of long bones and craniofacial bones, we opted to develop an

oral implant model system that would afford us with the ability to rigorously assess the program of oral implant osseointegration.

We first carried out a series of experiments in which implants were placed in the tibia. The surgical procedure, the osseointegration response, and the molecular and cellular characteristics of this process have been documented elsewhere [6,11,14,15,17,26,27]. Here, we show that new bone, originating from the tibial marrow cavity, is first evident on post-surgical day 5 (Supplemental Fig. 1A). The peri-implant bone is osseointegrated by day 7 (Supplemental Fig. 1B), and undergoes extensive remodeling at subsequent time points (Supplemental Fig. 1C–E).

We compared osseointegration in the tibia with osseointegration in the maxilla. Maxillary injuries were created immediately anterior to the first molar, along the alveolar crest in the edentulous space. After anesthesia, the oral cavity was rinsed with povidone–iodine solution (Fig. 2A) and a full thickness crestal incision was performed (Fig. 2B). The flap was raised and the alveolar bone was accessed (Fig. 2C). In an attempt to reduce trauma to the alveolar bone, a pilot hole was first created using a 0.3 mm drill, followed by a 0.45 mm drill (Fig. 2D). The implant (0.6 mm; Fig. 2E) was subsequently screwed into place (Fig. 2F). The gingival tissue was sutured in place, effectively enclosing the implant (Fig. 2G). The position of the implant was anterior to the first molar, along the edentulous ridge, perforating the sinus in all cases (Fig. 2H). After 14 days, the enclosed implant could be visualized through the tissue (Fig. 2I). Thus, the procedure used to place a murine oral implant was very similar to the procedure used for humans.

Murine oral implants undergo osseointegration

We first evaluated murine implants using histological analyses and found that within 7 days, there was evidence of bone formation in the peri-implant space (Fig. 3A). Upon close examination, the new bone appeared as an extension of the periosteal surfaces of the native maxillary bone (Fig. 3A′,A″). Fibroblasts also occupied the space between the cut edge of the bone and the implant surface (Fig. 3A′,A″). On day 14, more new bone was in contact with the implant surface (Fig. 3B, B′ and E). The new osteoid matrix was filled with vascular spaces (Fig. 3B″) and at this point the implant was clearly osseointegrated. The maximum amount of osseointegration was achieved by day 21 (Fig. 3E). Of 23 implants placed, 21 had primary stability and by histologic assessment, 17 achieved osseointegration (a 74% success rate).

Murine peri-implant tissue responses are similar to large animal responses

We evaluated the peri-implant tissue reaction to the surgery and implant placement, and focused on samples harvested on day 14, when implants had osseointegrated. The peri-implant mucosa appeared healthy and devoid of inflammatory cells (Fig. 4A). A junctional epithelium, composed of non-keratinized, invaginating epithelium had formed around the neck of a non-enclosed implant (Fig. 4A). The connective tissue attachment was well organized and was in direct contact with the implant surface (Fig. 4A). In regions closer to the native bone, new osteoid matrix was forming adjacent to the maxillary periosteum (arrows, Fig. 4A).

In mice, most implants projected through the maxillary bone into the olfactory epithelium (e.g., Fig. 3). Murine olfactory tissue, which is considerably larger in rodents, occupies the position of the nasal fossae in humans. We evaluated how these tissues responded to the implant. Fibroblasts had infiltrated the glandular olfactory epithelium and adhered to the implant without evidence of inflammation (Fig. 4B). In other cases, new bone formation was detectable in the fibrous tissue attached to the implant surface (Fig. 4B′).

Implant placement compromises osteocyte viability

We also analyzed cell viability in the maxillary bone. Using DAPI to detect cell nuclei and DIC to illustrate the osteocyte lacunae, we noted areas of extensive cell death in the cortical bone adjacent to the implant (dotted yellow line, Fig. 4C). The empty lacunae were exclusively found near the cut edge of the maxillary bone (dotted yellow line, Fig. 4C) and along the alveolar ridge where the flap was raised during the surgery (Fig. 4C′). This same DAPI staining indicated abundant new cells on the (unperturbed) nasal surface of the bone, along the new bone in contact with the implant surface, and along the periosteum (Fig. 4C,C′). Thus, the observed changes in peri-implant tissues are remarkably similar to the mucosal responses observed in large animals [28]. Furthermore, the results demonstrate how the standard surgical procedure of implant placement affects cell viability in the native bone.

Newly deposited peri-implant bone is distinct from lamellar bone of the intact cortex

We were particularly interested in the impact of the osteotomy on the viability of osteocytes in the maxillary bone, because this has implications for long-term bone regeneration and bone remodeling at the site of implant placement. Using samples from day 14, we first distinguished between mature osteocytes of the maxillary bone (dotted line, Figs. 5A,B) and new osteoid matrix: Mature maxillary bone had a lamellar organization whereas the new bone was characterized by a woven appearance (arrows, Figs. 5A,B). Aniline blue histology confirmed the lamellar organization of the maxillary bone (white dotted line, Figs. 5C,D) and the areas of new bone formation (arrows, Figs. 5C, D). Polarized light and Picrosirius red staining further demarcated the linear organization of the native bone (dotted line, Figs. 5E,F) from the crosshatched pattern seen in the new osteoid matrix (arrows, Figs. 5E, F). Thus, the structure of the new bone was woven in comparison to the lamellar organization of intact bone. We next evaluated the extent to which bone remodeling associated with implant placement affected these two osteoid matrices.

Robust bone turnover accompanies implant osseointegration

Using alkaline phosphatase (ALP) activity to identify newly mineralizing bone matrix [29,30] we found only the new bone exhibited ALP activity; native bone showed no evidence of ALP activity (dotted line indicates native bone, arrows indicate ALP activity in Figs. 5G,H).

The activity of osteoclasts, as measured by tartrate resistance acid phosphatase (TRAP) activity [31], was primarily evident on the remodeling surfaces of the new osteoid matrix, on both nasal and oral sides of the bone (Figs. 5I,J). TRAP activity was completely absent from the native maxillary cortex, indicating a very low rate of bone turnover.

TUNEL activity was used to identify cells undergoing apoptosis [32]. TUNEL activity was minimal along the implant surface on day 14, in keeping with the deposition of new bone here; instead, TUNEL^{+ve} cells were found in areas of the native lamellar bone (Fig. 5K), indicating osteocyte cell death in this locale. We used immunostaining for proliferating cell nuclear antigen (Fig. 5J) to confirm that cells continued to proliferate in the peri-implant space and in the lacunae (Fig. 5L). Immunostaining for Osteocalcin (Fig. 5M), Osteopontin (Fig. 5N), and Pro-collagen type I (Fig. 5O) verified that cells were actively differentiating into osteoblasts in the peri-implant space, and in the periosteum adjacent to the implant. Decorin (Fig. 5P) and Fibromodulin (Fig. 5Q), both markers of fibroblastic cells, were not expressed in the gap-interface, thus confirming that bone, and not fibrous tissue, formed in the peri-implant space.

Discussion

Maxillary healing is more challenging than long bone healing

Many of our assumptions concerning oral implant osseointegration are extrapolated from experimental models studying skeletal tissue repair in long bones [33,34]. We avoided this presupposition by directly studying oral implant osseointegration in an oral bone, the maxilla. First, we showed that in comparison to long bone injuries, craniofacial bones are derived from cranial neural crest (Fig. 1). Second, we find that injuries to craniofacial bones tended to heal more slowly than analogous injuries to the tibia (Fig. 1). The reasons for this are not obvious but there are a number of other features that undoubtedly contribute to the difference in healing potential: for example, the marrow space in the tibia contains abundant numbers of osteoprogenitor cells, a robust blood supply, and stem cell niche signals [35,36], all of which are essential for new bone formation. The maxillary bone, however, has little or no marrow space and presumably lacks the stem cell populations that reside in the marrow cavity. The mechanical environment is also different between long bones and craniofacial bones, and physical forces play an important role in implant osseointegration [14]. However, characterizing the relevant mechanical forces, and their relative impact on healing potential is beyond the scope of this paper. Whatever the causal factors are, our study demonstrated that even when small injuries are made in the maxilla, they fail to heal with new bone (Fig. 1), and thus represent a “critical size” skeletal defect (e.g., see [37,38]). Collectively, these data strongly suggest that in order to understand and improve the process of oral implant osseointegration, the most relevant studies will take this healing potential difference into account.

The peri-implant mucosal response is similar in mice and large animals

Establishing contact between the mucosa and the implant creates an effective barrier against bacterial invasion into the soft tissues, and therefore protects the bone. In our mouse model, we observed three tissue compartments in contact with the implant: a gingival epithelial zone, a connective tissue zone, and a periosteal zone (Fig. 4). These same zones have been described in large animal models [28], and thus this murine model recapitulates this important feature of implant biology.

This murine model also can be used for studying how surface and shape modifications to the neck of the implant, or the connector, affect the adhesion of the connective tissue fibroblasts in vivo. Similar studies have been conducted in dogs [39], but mice offer a wide array of molecular and cellular tools with which to analyze the cellular and tissue-level responses that are unavailable for canine species. Other groups [19–21] have used rodents with similar maxillary models, where implant is placed in a ridge defect model where a tooth never existed. Collectively, these studies and ours show that oral implant osseointegration is achievable in a rodent model.

The chronology of osseointegration is similar in mice and large animals

The surgical procedure used in mice parallels the general procedure used for implant placement in humans [40,41], but there are two general features that differ between humans and the mouse model that may have a bearing on osseointegration. First, there is a difference in skeletal architecture in the maxilla: in mice, there is a reduced amount of trabecular (cancellous) bone and in place of this trabecular framework is cortical bone (Fig. 3). Cortical bone provides primary stability for implants [42] whereas the function(s) of the trabecular bone in osseointegration is unknown. The marrow that occupies the trabecular bone in humans may be the source of growth factors that stimulate new bone deposition, which in turn might influence the extent of osseointegration, but this point remains conjecture. A second point distinguishing osseointegration in mice from that in humans is the rapidity with which implant osseointegration occurs in mice. In humans, osseointegration is thought to take at least 6–8 weeks [2]. In our mouse model, implant osseointegration is evident by day 14 (Fig. 3). The similarities between this mouse model and large animal models of osseointegration allowed us to explore the molecular and cellular characteristics that affect implant osseointegration.

The periosteum is the likely source of osteogenic stem cells that give rise to peri-implant bone

Abundant new bone forms around maxillary implants (Fig. 3) but the source(s) of the osteoblasts are not currently known. Because there is no obvious marrow space in the murine maxillae, we speculated that the new bone arises from the nasal and oral periostea of the maxilla (Fig. 5A). Implant bed preparation injures the periosteum, and the typical response to such an injury is cell proliferation in the fibrous layer [14]. In a mechanically neutral environment, these proliferating skeletal progenitor cells differentiate into osteoblasts and give rise to new bone [23]. Consequently, all efforts should be made to preserve the periosteum at the site of implant placement because in this tissue resides the skeletal stem cells that generate the new bone [22].

Implant placement destroys osteocytes in the cortical bone

A finding from these analyses that has direct clinical relevance was the extensive cell death observed in the alveolar bone in response to the implant surgery, and the cell death in the crest of the cortical bone in response to the raised flap (Figs. 4,5). In both cases, only the mineralized matrix of the dead bone is retained and it provides some mechanical support for the implant. The dead bone must eventually be resorbed by osteoclasts, and replaced by new bone (e.g., see [43]). This process of cortical bone remodeling does not take place

immediately (Fig. 2) but rather, appears to be part of the normal bone turnover process. In humans, this bone turnover is measured in years [44]; in mice, this bone turnover is measured in months. In this window of time, between TRAP-mediated bone resorption and ALP^{+ve} new bone formation, the implant may lose some of its stability [45]. The same cycle of bone resorption and bone formation likely occurs in humans, and a key consideration for the timing of prosthetic loading will undoubtedly be this phase of peri-implant bone turnover.

Towards predicting successful implant osseointegration

Canine models of oral implant osseointegration have been extensively employed in the past, and have a significant advantage because human size implants can be directly tested in a dog model. There are a number of serious limitations, however, including the cost associated with a large study in canines and the complete lack of genetic, molecular and cellular tools for analyses. Once the small size of the mouse is overcome, there are a number of advantages to this model of oral implant osseointegration. Our long-term objective is to be able to predict implant success versus failure by careful analysis of the steps leading up to new bone formation around implants. A step towards achieving that goal is the development of a mouse model whereby the program of implant osseointegration can be rigorously dissected. Future studies will focus on the basic biology of implant failure, as well as new therapeutic strategies to re-program fibrous tissue around a failed implant into the bone.

Supplementary Material

Refer to Web version on PubMed Central for supplementary material.

Acknowledgments

We would like to thank Du Cheng for developing smartphone microscope adaptation device, which allowed us to take intra-oral photographs during murine surgeries.

Source of funding statement: This research project was supported by a grant from the California Institute of Regenerative Medicine (CIRM) TR1-01249 to J.A.H. and a CIRM scholar award TB1-01190 to D.J.H.

References

1. Narby B, Kronstrom M, Soderfeldt B, Palmqvist S. Changes in attitudes toward desire for implant treatment: a longitudinal study of a middle-aged and older Swedish population. Int J Prosthodont. 2008; 21:481–5. [PubMed: 19149061]
2. Esposito M, Grusovin MG, Willings M, Coulthard P, Worthington HV. The effectiveness of immediate, early, and conventional loading of dental implants: a Cochrane systematic review of randomized controlled clinical trials. Int J Oral Maxillofac Implants. 2007; 22:893–904. [PubMed: 18271370]
3. Wennerberg A, Albrektsson T. Effects of titanium surface topography on bone integration: a systematic review. Clin Oral Implants Res. 2009; 20(Suppl. 4):172–84. [PubMed: 19663964]
4. Ding X, Liao SH, Zhu XH, Zhang XH, Zhang L. Effect of diameter and length on stress distribution of the alveolar crest around immediate loading implants. Clin Implant Dent Relat Res. 2009; 11:279–87. [PubMed: 18783411]
5. Wikesjo UM, Polimeni G, Qahash M. Tissue engineering with recombinant human bone morphogenetic protein-2 for alveolar augmentation and oral implant osseointegration: experimental

observations and clinical perspectives. Clin Implant Dent Relat Res. 2005; 7:112–9. [PubMed: 15996358]

6. Popelut A, Rooker SM, Leucht P, Medio M, Brunski JB, Helms JA. The acceleration of implant osseointegration by liposomal Wnt3a. Biomaterials. 2010; 31:9173–81. [PubMed: 20864159]
7. Yan SG, Zhang J, Tu QS, Ye JH, Luo E, Schuler M, et al. Enhanced osseointegration of titanium implant through the local delivery of transcription factor SATB2. Biomaterials. 2011; 32:8676–83. [PubMed: 21862122]
8. Sennerby L, Thomsen P, Ericson LE. Early tissue response to titanium implants inserted in rabbit cortical bone. Part I. Light microscopic observations. J Mater Sci Mater Med. 1993; 4:240–50.
9. de Barros AP, Takiya CM, Garzoni LR, Leal-Ferreira ML, Dutra HS, Chiarini LB, et al. Osteoblasts and bone marrow mesenchymal stromal cells control hematopoietic stem cell migration and proliferation in 3D in vitro model. PLoS One. 2010; 5:e9093. [PubMed: 20161704]
10. Leucht P, Kim JB, Currey JA, Brunski J, Helms JA. FAK-mediated mechanotransduction in skeletal regeneration. PLoS One. 2007; 2:e390. [PubMed: 17460757]
11. Colnot C, Romero DM, Huang S, Rahman J, Currey JA, Nanci A, et al. Molecular analysis of healing at a bone–implant interface. J Dent Res. 2007; 86:862–7. [PubMed: 17720856]
12. Currey, JA.; D'Anjou, C.; Leucht, P.; Wazen, R.; Helms, JA.; Nanci, A., et al. Determination of/in vivo/mechanical properties of healing interfacial tissue at an implant site in bone; 2nd international conference on mechanics of biomaterials & tissues; Lihue, Kaua'I, Hawaii. 2007. [abstract 039]
13. D'Anjou, C.; Currey, JA.; Wazen, R.; Nanci, A.; Leucht, P.; Helms, JA., et al. Stiffness of the bone implant interface as an indicator of bone healing; 53rd annual orthopedic research society; San Diego, CA. 2007.
14. Leucht P, Kim JB, Wazen R, Currey JA, Nanci A, Brunski JB, et al. Effect of mechanical stimuli on skeletal regeneration around implants. Bone. 2007; 40:919–30. [PubMed: 17175211]
15. Wazen RM, Currey JA, Guo H, Brunski JB, Helms JA, Nanci A. Micromotion-induced strain fields influence early stages of repair at bone–implant interfaces. Acta Biomater. 2013; 9:6663–74. [PubMed: 23337705]
16. Temiyasathit S, Tang WJ, Leucht P, Anderson CT, Monica SD, Castillo AB, et al. Mechanosensing by the primary cilium: deletion of Kif3A reduces bone formation due to loading. PLoS One. 2012; 7:e33368. [PubMed: 22428034]
17. Leucht P, Monica SD, Temiyasathit S, Lenton K, Manu A, Longaker MT, et al. Primary cilia act as mechanosensors during bone healing around an implant. Med Eng Phys. 2012; 3:392–402. [PubMed: 22784673]
18. services USDoHaH. , editor. Quality AfHRa. Number of patients, number of procedures, average patient age, average length of stay—national hospital discharge survey 1999–2003. U.S. Department of Health and Human Services; 1999. current
19. Dunn CA, Jin Q, Taba M Jr, Franceschi RT, Bruce Rutherford R, Giannobile WV. BMP gene delivery for alveolar bone engineering at dental implant defects. Mol Ther. 2005; 11:294–9. [PubMed: 15668141]
20. Karimbux NY, Sirakian A, Weber HP, Nishimura I. A new animal model for molecular biological analysis of the implant–tissue interface: spatial expression of type XII collagen mRNA around a titanium oral implant. J Oral Implantol. 1995; 21:107–13. [discussion 114–5]. [PubMed: 8699501]
21. Lin Z, Rios HF, Volk SL, Sugai JV, Jin Q, Giannobile WV. Gene expression dynamics during bone healing and osseointegration. J Periodontol. 2011; 82:1007–17. [PubMed: 21142982]
22. Chan CK, Chen CC, Luppen CA, Kim JB, DeBoer AT, Wei K, et al. Endochondral ossification is required for haematopoietic stem-cell niche formation. Nature. 2009; 457:490–4. [PubMed: 19078959]
23. Leucht P, Kim JB, Amasha R, James AW, Girod S, Helms JA. Embryonic origin and Hox status determine progenitor cell fate during adult bone regeneration. Development. 2008; 135:2845–54. [PubMed: 18653558]
24. Echelard Y, Vassileva G, McMahon AP. Cis-acting regulatory sequences governing Wnt-1 expression in the developing mouse CNS. Development. 1994; 120:2213–24. [PubMed: 7925022]
25. Helms JA, Amasha RR, Leucht P. Bone voyage: an expedition into the molecular and cellular parameters affecting bone graft fate. Bone. 2007; 41:479–85. [PubMed: 17692586]

26. Brunski, J.; Glantz, P-O.; Helms, JA.; Nanci, A. Transfer of mechanical load across the interface. In: Branemark, P-I., editor. The osseointegration book. Berlin: Quintessenz Verlags-GmbH; 2005. p. 209-49.
27. Kim JB, Leucht P, Currey JA, Brunski J, Helms JA. FAK-mediated mechanotransduction in skeletal regeneration. PLoS One. 2007; 2:e390. [PubMed: 17460757]
28. Berglundh T, Abrahamsson I, Welander M, Lang NP, Lindhe J. Morphogenesis of the peri-implant mucosa: an experimental study in dogs. Clin Oral Implants Res. 2007; 18:1–8. [PubMed: 17224016]
29. Weinreb M, Shinar D, Rodan GA. Different pattern of alkaline phosphatase, osteopontin, and osteocalcin expression in developing rat bone visualized by in situ hybridization. J Bone Miner Res. 1990; 5:831–42. [PubMed: 2239367]
30. Stucki U, Schmid J, Hammerle CF, Lang NP. Temporal and local appearance of alkaline phosphatase activity in early stages of guided bone regeneration. A descriptive histochemical study in humans. Clin Oral Implants Res. 2001; 12:121–7. [PubMed: 11251661]
31. Ashton BA, Ashton IK, Marshall MJ, Butler RC. Localisation of vitronectin receptor immunoreactivity and tartrate resistant acid phosphatase activity in synovium from patients with inflammatory or degenerative arthritis. Ann Rheum Dis. 1993; 52:133–7. [PubMed: 7680551]
32. Mori C, Nakamura N, Okamoto Y, Osawa M, Shiota K. Cytochemical identification of programmed cell death in the fusing fetal mouse palate by specific labelling of DNA fragmentation. Anat Embryol. 1994; 190:21–8. [PubMed: 7527193]
33. Clokie CM, Warshawsky H. Morphologic and radioautographic studies of bone formation in relation to titanium implants using the rat tibia as a model. Int J Oral Maxillofac Implants. 1995; 10:155–65. [PubMed: 7744434]
34. Thalji G, Gretzer C, Cooper LF. Comparative molecular assessment of early osseointegration in implant-adherent cells. Bone. 2012; 52:444–53. [PubMed: 22884725]
35. Yin T, Li L. The stem cell niches in bone. J Clin Invest. 2006; 116:1195–201. [PubMed: 16670760]
36. Herzog EL, Chai L, Krause DS. Plasticity of marrow-derived stem cells. Blood. 2003; 102:3483–93. [PubMed: 12893756]
37. Cooper GM, Mooney MP, Gosain AK, Campbell PG, Losee JE, Huard J. Testing the critical size in calvarial bone defects: revisiting the concept of a critical-size defect. Plast Reconstr Surg. 2010; 125:1685–92. [PubMed: 20517092]
38. Schmitz JP, Hollinger JO. The critical size defect as an experimental model for craniomandibulofacial nonunions. Clin Orthop Relat Res. 1986:299–308. [PubMed: 3084153]
39. Linkevicius T, Apse P. Influence of abutment material on stability of peri-implant tissues: a systematic review. Int J Oral Maxillofac Implants. 2008; 23:449–56. [PubMed: 18700367]
40. Branemark PI, Adell R, Breine U, Hansson BO, Lindstrom J, Ohlsson A. Intra-osseous anchorage of dental prostheses. I Experimental studies. Scand J Plast Reconstr Surg. 1969; 3:81–100. [PubMed: 4924041]
41. Buser D, Martin W, Belser UC. Optimizing esthetics for implant restorations in the anterior maxilla: anatomic and surgical considerations. Int J Oral Maxillofac Implants. 2004; (19 Suppl): 43–61. [PubMed: 15635945]
42. Hong J, Lim YJ, Park SO. Quantitative biomechanical analysis of the influence of the cortical bone and implant length on primary stability. Clin Oral Implants Res. 2012; 23:1193–7. [PubMed: 22092387]
43. Haga M, Fujii N, Nozawa-Inoue K, Nomura S, Oda K, Uoshima K, et al. Detailed process of bone remodeling after achievement of osseointegration in a rat implantation model. Anat Rec (Hoboken). 2009; 292:38–47. [PubMed: 18727113]
44. Clarke B. Normal bone anatomy and physiology. Clin J Am Soc Nephrol. 2008; 3(Suppl. 3):S131–9. [PubMed: 18988698]
45. Raghavendra S, Wood MC, Taylor TD. Early wound healing around endosseous implants: a review of the literature. Int J Oral Maxillofac Implants. 2005; 20:425–31. [PubMed: 15973954]

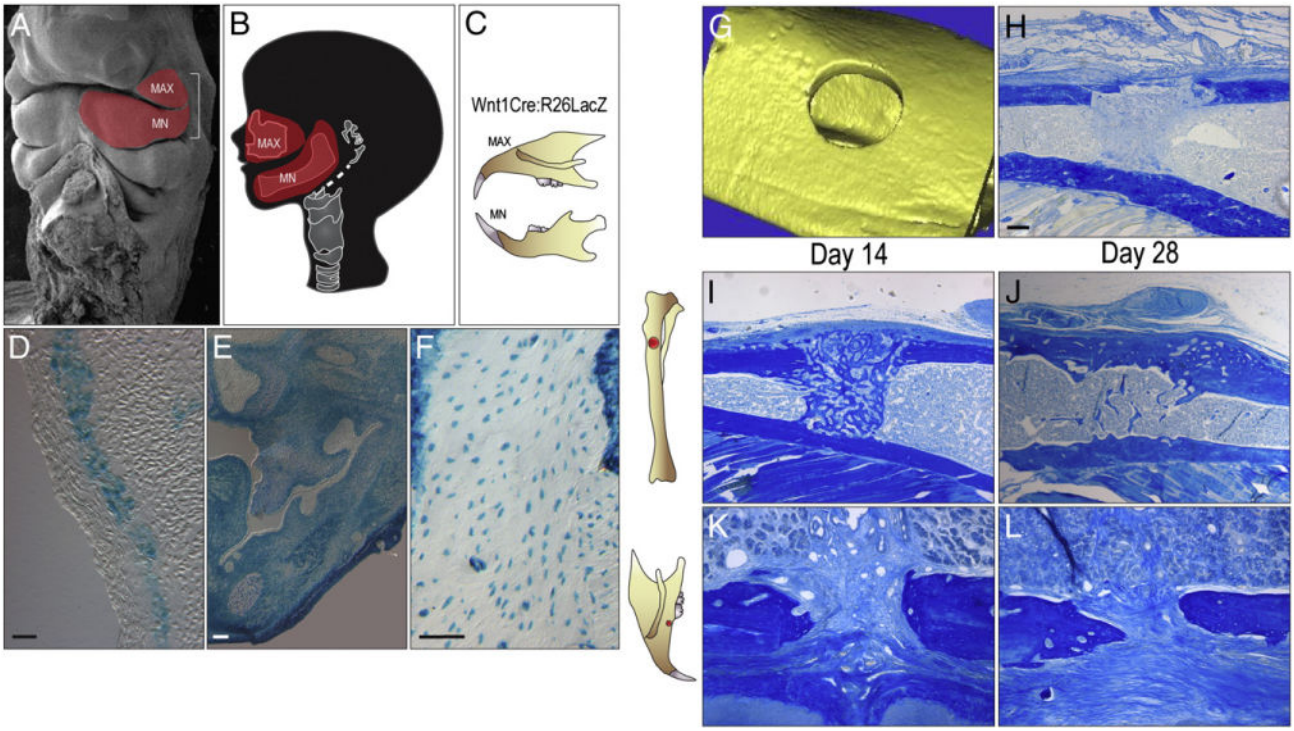

Fig. 1.

Robust bone repair and implant osseointegration in the tibia compared to the maxilla. (A) Scanning electron micrograph of embryonic head; the red region indicates cranial neural crest cells of the first branchial arch, (B) that later develop into the maxilla and the mandible. (C) The cranial neural crest cells of Wnt1Cre:R26RLacZ mice are permanently labeled. (D) Permanently labeled LacZ + cranial neural crest cells are found within the first branchial arch along with (E) many dental tissues. (F) Mature osteocytes of the maxilla are also permanently marked for their cranial neural crest origin. (G) Micro-CT image of 0.8 mm skeletal defect created in mesoderm-derived long bone, the tibia. (H) Representative tissue section through a 0.8 mm tibial defect following injury, stained with aniline blue. (I) Representative tissue section through a 0.8 mm tibial defect on post-surgery day 14, stained with aniline blue. The dark blue color denotes collagen-rich matrix in the defect site. (J) Representative section on post-surgery day 28 from the tibia implant site. (K) Representative tissue section through a 0.6 mm maxillary defect on post-surgery day 14, stained with aniline blue. The dark blue color indicates the collagen-rich matrix of the bone. (L) Aniline blue stain of the maxillary defect on post-surgery day 28. MAX, maxilla; MN, mandible. Scale bars: (D–F), 100 μm; (H–L) 100 μm.

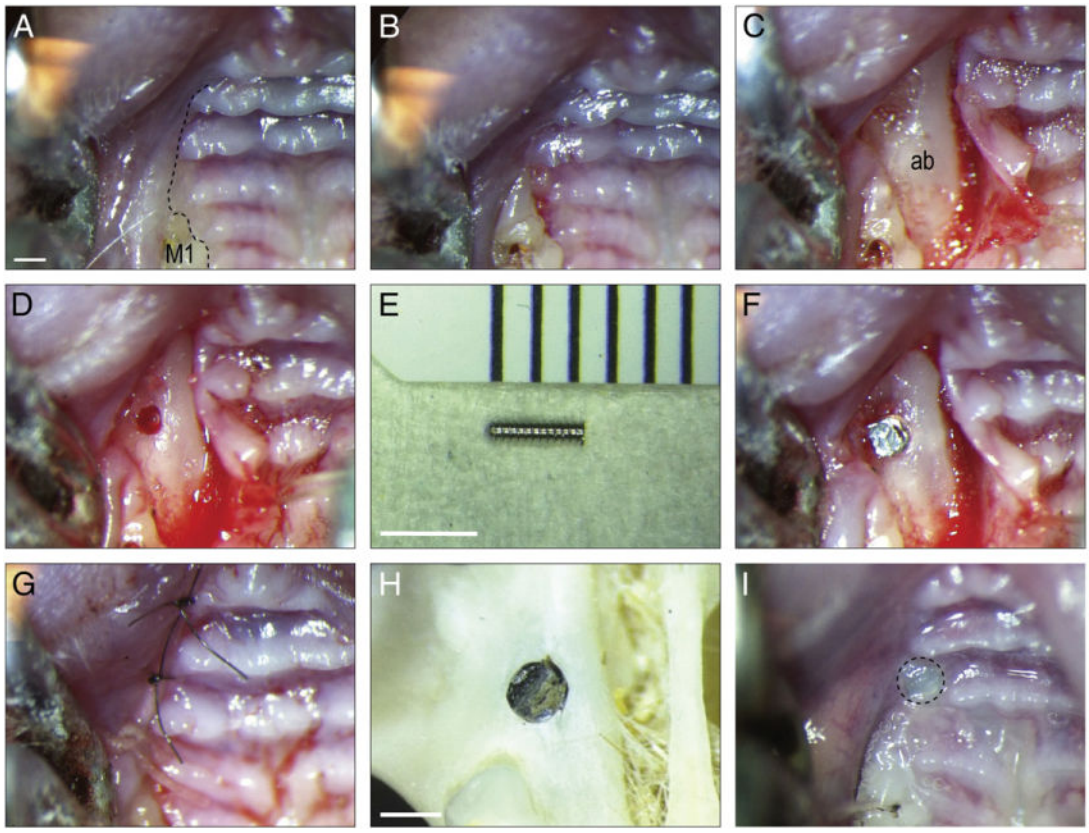

Fig. 2.

An oral implant model in mice. (A) Pre-operative photograph of the alveolar crest, anterior to the maxillary first molar; black dotted line indicates incision placement. (B) The intrasulcular incision extends from the lingual surface of the maxillary first molar anteriorly, to the crest of the edentulous space. (C) A full-thickness flap is elevated to expose the alveolar bone. (D) A 0.45 mm hole is prepared on the crest, 1.5 mm anterior of the first maxillary molar. (E) The 0.6 mm diameter titanium alloy implant. (F) The implant is placed manually, followed by careful rinsing. (G) Wounds are closed with non-absorbable single interrupted sutures. (H) Skeletal preparation showing location of the maxillary implant relative to the dentition and bones of the skull. (I) Soft tissue covered the healing implant days post-surgery. M1, maxilla first molar; ab, alveolar bone. Scale bars: (A–D, G, I) 600 μm; (E) 2500 μm; (H) 500 μm.

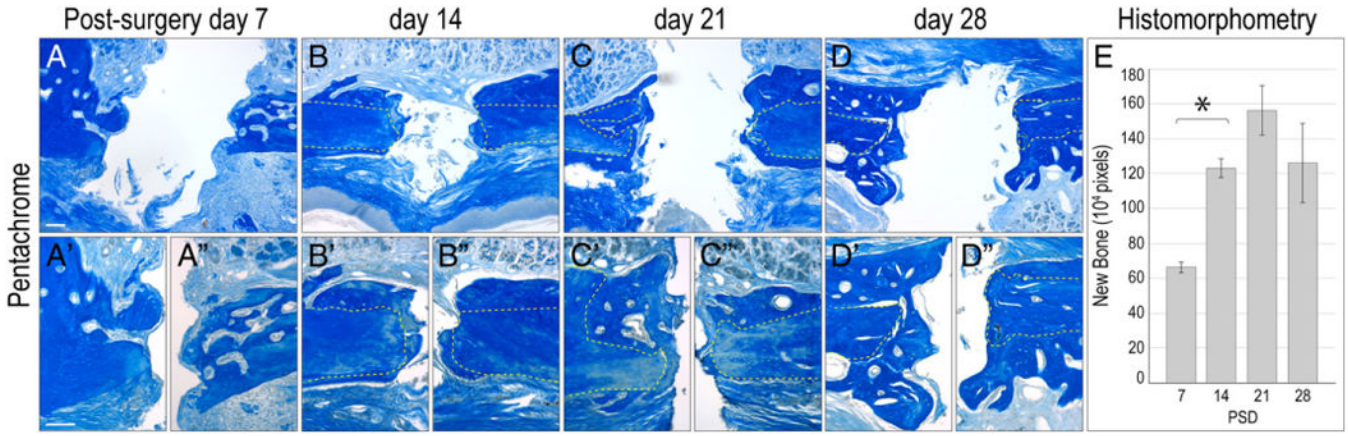

Fig. 3.

Chronology of implant osseointegration in the oral cavity. (A) Representative sagittal tissue section through a maxilla implant site on post-surgery day 7, stained with aniline blue. The blue color denotes collagen-rich matrix in the defect site. (A′ and A″) High magnification images of the bone in contact with the implant; white dotted lines outline original bone. (B) Maxilla implant site on post-surgery day 14. (B′ and B″) High magnification image of the bone in contact with the implant. (C) Representative sagittal tissue section through a maxillary implant. (C′ and C″) High magnification images on post-surgery day 21. (D) Representative sagittal tissue section through a maxillary implant site on post-surgery day 28, stained with aniline blue. (D′ and D″) High magnification image of the bone in contact with the implant. (E) The amount of new bone on post-surgery days 7, 14, 21, and 28 was quantified using histomorphometric measurements. Scale bars: (A–D) 200 μm; (A′–D″) 50 μm. Results are presented as the mean ± SEM. $P \leq 0.01$ was considered to be significant.

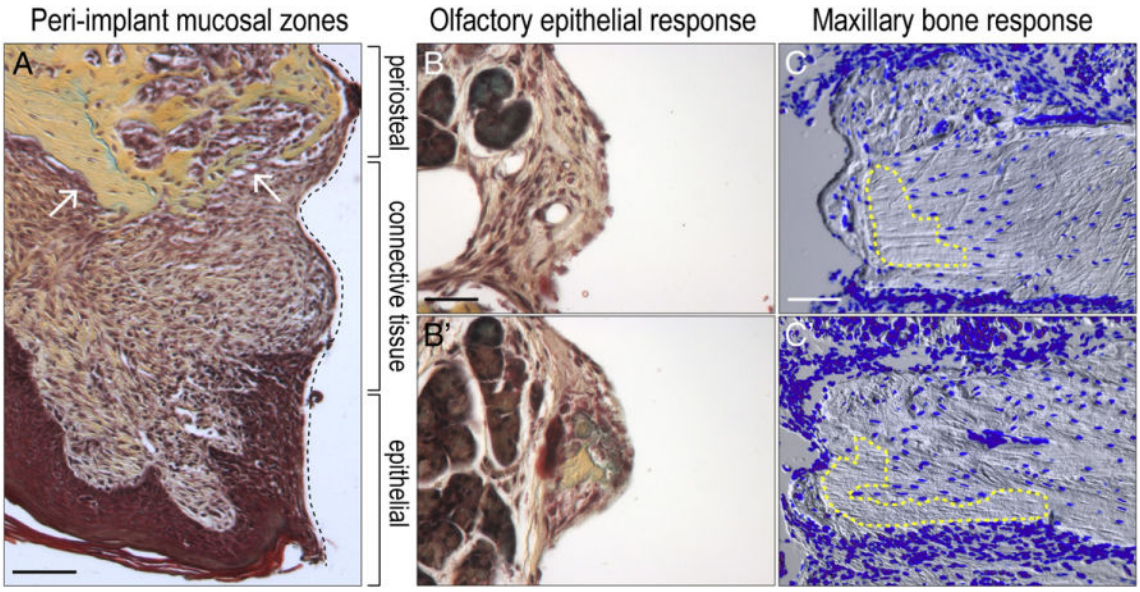

Fig. 4.

Peri-implant tissue responses to the implant. (A) Representative sagittal tissue section through a maxilla implant site on post-surgery day 14, stained with Pentachrome. Organization of the peri-implant mucosa into three zones; black dotted line indicates tissue–implant interface. White arrows point to periosteal response. (B and B′) High magnification images of representative sagittal tissue sections through a maxillary implant site on post-surgery day 14, stained with Pentachrome. Note the olfactory tissue adjacent to the implant surface and the presence of new bone within the fibrous component of the tissue. (C and C′) Representative sagittal tissue sections through a maxillary implant site on post-surgery day 14, stained with DAPI; blue indicates cell nuclei. Yellow dotted regions indicate areas of cell death. Scale bars: (A) 200 μm; (B–B′) 50 μm; (C–C′) 200 μm.

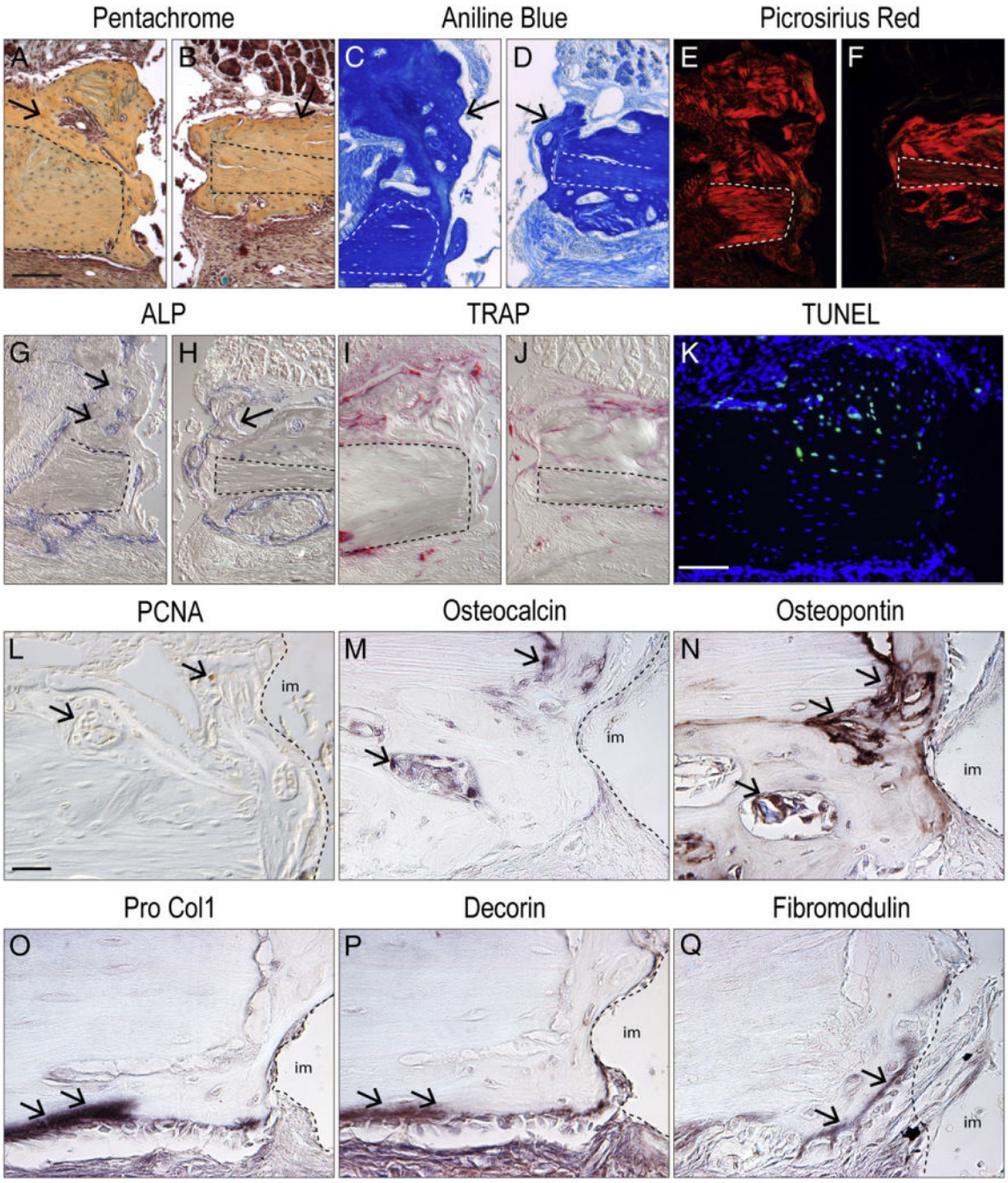

Fig. 5.

Cellular and molecular analyses of oral implant osseointegration. (A and B) Representative sagittal tissue section through a maxillary implant site on post-surgery day 14, stained with Pentachrome; dotted line indicates native bone and arrows indicate new bone. (C and D) aniline blue stain, the dark blue color denotes collagen in the osteoid tissue. (E and F) Picrosirius red stain, observed with polarized light; the red color denotes the orientation of the collagen. (G and H) Alkaline phosphatase (ALP) activity is detectable in the newly mineralizing bone matrix. (I and J) Tartrate resistance acid phosphatase (TRAP) staining is evident around newly formed bone. (K) TUNEL staining and DAPI, observed with

fluorescent light, where the blue color denotes nuclei of the cells and green color denotes cells undergoing apoptosis. (L) Representative sagittal tissue section of the maxillary implant site on post-surgery day 14 immunostained for immunostained for Proliferating Cell Nuclear Antigen (PCNA); arrows indicate positive stain. (M) Representative sagittal tissue section of the maxillary implant site on post-surgery day 14, immunostained for Osteocalcin. (N) Representative sagittal tissue section of the maxillary implant site on post-surgery day 14, immunostained for Osteopon-tin. (O) Representative sagittal tissue section of the front maxilla implant site on post-surgery day 14 immunostained for Pro-Collagen 1. (P) Representative sagittal tissue section of the front maxillary implant site on post-surgery day 14, immunostained for Decorin. (Q) Representative sagittal tissue sections from the front maxillary implant site on post-surgery day 14, immunostained for fibromodulin. Scale bars: (A–K) 100 μm; (L–Q) 25 μm.